ARTICLE
Translational Therapeutics

The role of anlotinib-mediated EGFR blockade in a positive feedback loop of CXCL11-EGF-EGFR signalling in anaplastic thyroid cancer angiogenesis

Juyong Liang [1], Zhijian Jin [1], Jie Kuang [1], Haoran Feng[1], Qiwu Zhao [1], Zheyu Yang[1], Ling Zhan[1], Baiyong Shen[1], Jiqi Yan[1], Wei Cai [1], Xi Cheng [1] and Weihua Qiu [1]

BACKGROUND: Hypoxia-induced angiogenesis functions importantly in anaplastic thyroid cancer (ATC) progression. However, the therapeutic potential of broad-spectrum anti-angiogenic agent remains undefined. Anlotinib conventionally targets VEGFR, FGFR and PDGFR. Here, a novel role of anlotinib on ATC angiogenesis was illustrated.
METHODS: Molecular expressions were established via tissue microarray. Multiple assays (tubule formation, 3D sprouting and chicken chorioallantoic membrane model) were used for angiogenic evaluation. Panels of molecular screening were achieved by antibody and PCR arrays. The loop binding motif of EGFR for homology modelling was prepared using Maestro.
RESULTS: Anlotinib could dose- and time-dependently inhibit cell viability under normoxia and hypoxia and could repress hypoxia-activated angiogenesis more efficiently in vitro and in vivo. CXCL11 and phospho-EGFR were hypoxia-upregulated with a positive correlation. The cancer–endothelium crosstalk could be mediated by the positive CXCL11-EGF-EGFR feedback loop, which could be blocked by anlotinib directly targeting EGFR *via* a dual mechanism by simultaneous inhibitory effects on cancer and endothelial cells. The AKT-mTOR pathway was involved in this regulatory network.
CONCLUSIONS: The newly identified CXCL11-EGF-EGFR signalling provided mechanistic insight into the interaction between cancer and endothelial cells under hypoxia, and EGFR was a novel target. Anlotinib may be the encouraging therapeutic candidate in ATC.

BACKGROUND
Thyroid cancer is the most prevalent endocrine malignancy with increasing incidence.[1] Although anaplastic thyroid cancer (ATC) accounts for only 1–2% of all thyroid cancers, it is responsible for the majority of thyroid cancer-related deaths due to high aggressiveness.[2] Unlike differentiated thyroid cancer, ATC is resistant to surgical, chemical and isotopic interventions.[3] Insufficient survival improvement has been reported even with targeted therapies.[4,5]

ATC progression depends on angiogenic signalling,[6] which is promoted by hypoxic stress.[7] Hypoxia-induced angiogenesis is the major survival gateway for malignancies.[8] Hypoxia-inducible factor 1α (HIF1α) is the key regulator of the oxygen response and the focal point of converging pathways that mediate the crosstalk between the tumour and vascular cells.[9–11] HIF1α stabilisation and upregulation of its downstream proangiogenic factors, including VEGF, EGF, CCL- and CXCL-chemokines, bridge the intercellular communications.[12]

Accumulating evidence suggests the importance of anti-angiogenic therapy in ATC treatment based on the critical role of neovascularisation in thyroid carcinogenesis.[13] A number of angiogenic inhibitors have achieved favourable therapeutic effects; however, the long-term prognosis remains unsatisfactory.[6,14] These limitations may be partially due to the complex feedback of angiogenic signalling that induces eventual tumour adaptation.[15] Therefore, the broad-spectrum agents may be encouraging therapeutic candidates. Anlotinib, a novel multiple-targeted receptor tyrosine kinase (RTK) inhibitor, can primarily block VEGF/PDGF/FGF-induced angiogenesis.[16] The current study aimed to explore the role of anlotinib in the regulatory network of hypoxia-induced angiogenesis in ATC.

METHODS
Tissue microarray and immunohistochemistry (IHC) scoring
Formalin-fixed paraffin-embedded tissue microarray included 60 specimens from 30 patients. However, due to specimens and staining missing, five patients were excluded. Finally, a total of 50 specimens (tumour and peritumour) from 25 patients were used in this study. All cases were diagnosed by the pathologist, and IHC images were also evaluated by the pathologist. IHC scoring was completed according to the percentage of positive cells (0 = 0–5%, 1 = 5–25%, 2 = 26–50%, 3 = 51–75%, 4 = 76–100%) and the staining intensity (0 = negative, 1 = weak, 2 = moderate, 3 = strong). The two scores were multiplied to generate an immunoreactive score ranging from 0 to 12.[17]

[1]Department of General Surgery, Ruijin Hospital, Shanghai Jiao Tong University School of Medicine, Shanghai, China
Correspondence: Wei Cai (caiwei@shsmu.edu.cn) or Xi Cheng (drchengxi@126.com) or Weihua Qiu (qwh11072@rjh.com.cn)
These authors contributed equally: Juyong Liang, Zhijian Jin, Jie Kuang

The role of anlotinib-mediated EGFR blockade in a positive feedback loop...
J Liang et al.

391

Cell culture and reagents

Normal human thyroid epithelium cell line (Nthy-ori 3–1) and human umbilical vein endothelial cell line (HUVEC) were purchased from China Center for Type Culture Collection (Wuhan, China). Human ATC cell lines BCPAP, BHT101, KHM-5M, C643 and CAL-62 were obtained from ATCC (Rockville, MD). All cell lines were authenticated by STR/DNA profiling by BIOWING BIOTECH-NOLOGY (Shanghai, China). Nthy-ori 3–1, BCPAP, KHM-5M and C643 were cultured in RPMI-1640 with 10% foetal bovine serum (FBS, Gibco, USA). CAL-62 and BHT101 were cultured in DMEM with 10% FBS. HUVEC was cultured in ECM (Sciencell, USA). Antibiotics were added to media formulations. Cells were cultured at 37 °C in 5% CO_2 either under normoxia ($O_2 = 20\%$) or hypoxia ($O_2 = 2\%$). All cells were preserved at -80 °C using CELLSAVING (New Cell & Molecular Biotech, China). Anlotinib was obtained from CHIA TAI TIANQING PHARMACEUTICAL GROUP Co. Ltd. (Jiangsu, China), dissolved in PBS and diluted with medium to the desired concentration. Gefitinib was purchased from Selleck Chemicals (Houston, TX). Recombinant human CXCL11 (rhCXCL11) and recombinant human HB-EGF (rhEGF) were from PeproTech (USA). The human CXCL11 neutralising antibody (anti-CXCL11) was gained from R&D Systems, Inc.

CCK-8 assay

CCK-8 assay (Dojindo, Japan) was utilised to confirm the cytotoxicity of anlotinib on ATC cells. Cells were plated at 5000 cells and were treated with anlotinib at 0, 0.5, 1, 2, 5, 10, 20, and 40 μM for 24, 48 or 72 h under normoxia or hypoxia. At the test point, 100 μl CCK-8 was added and then the OD was detected by spectrophotometer. Similarly, the viability of HUVEC was examined using CCK-8 as well.

Colony-formation assay

ATC cells (1000 per well) were seeded in six-well plates under normoxia or hypoxia for 2 weeks. At the end of the first week, anlotinib (5 μM) was added to the treatment groups. In the second week, the colonies were stained by 0.1% crystal violet for 30 min.

Apoptosis assay

ATC cells were treated with anlotinib (1 μM) for 24 h under normoxia or hypoxia, respectively. Their supernatants were collected to intervene the HUVEC for 24 h. The Annexin V-FITC Apoptosis Detection kit (BD Pharmingen, USA) was used for apoptotic analysis. HUVEC were harvested and washed twice with PBS. Following the suspension with 100 μl of binding buffer, samples were stained with 3 μl Annexin V-FITC and 5 μl propidium iodide (PI) and incubated at room temperature for 15 min in the dark. Finally, 300 μl of binding buffer was added to each sample. The apoptotic rate was analysed by flow cytometry using the FACS Calibur system (BD Biosciences, USA). Data were obtained from three independent experiments.

Endothelial tubule formation assay

Ninety-six-well plates were pre-coated with 50 μL Matrigel (Biocoat, Corning) at 37 °C for 1 h. After treatment, HUVEC were incubated at a density of 2×10^4 cells per well for 6 h. Tubule images were analysed by Image-Pro Plus software and quantified by the tubule length. Data were obtained from three independent experiments.

Migration assay

Migration assay was performed using Transwell Permeable Supports (CLP, Corning). Serum-free medium (200 μL) containing 1×10^5 HUVEC was added to the upper chamber, and 800 μL of tumour supernatants were added to the lower chamber. After incubation of 24 or 48 h, cells were stained with 0.1% crystal violet for 30 min. The number of migrating cells was normalised to the number of total cells and was calculated per microscopic field. The mean number was estimated by counting average cells in five visual fields of three independent experiments.

3D sprouting assay

The sprouting assay was performed as described previously.[18] Rat tail tendon collagen Type I was acquired from Xinyou Biotechnology Co., Ltd (Hangzhou, China). Collagen was prepared at pH 7.0 and at a concentration of 2 mg/ml. We added 100 μl of collagen into the six-well plates. A suspension containing HUVEC (80,000) was seeded around the polymerised collagen matrices. Following the incubation of 800 μl medium, HUVEC was allowed to sprout overnight. Later, cells were fixed using 3% glutaraldehyde (Sigma-Aldrich) and stained by 0.1% toluidine blue (Sigma-Aldrich). The sprouting number was normalised to the number of total cells. Data were obtained from three independent experiments.

Chicken chorioallantoic membrane (CAM) model

The egg was hatched in 37 °C for 7 days. A round window (1 cm in diameter) was made. The filter paper was placed on the egg, and then 30 μL of tumour supernatant was dropped onto the filter paper tray, which was sealed with a transparent tape for three days. On day 10, eggs were photographed with a MacroPATH dissecting microscope (Milestone, Italy).

Generation of gene overexpression and knockdown cells

Lentivirus for CXCL11 and EGFR overexpression was purchased from Shanghai Bioegene Co. Ltd. (Shanghai, China). Gene knockdown of EGFR, CXCL11, CXCR3 and CXCR7 was achieved by siRNA. Sense and anti-sense sequences were showed in Supplementary Table 1. Transfection was performed as described before.[17] After cells were seeded into six-well plates at 80% concentration, plasmids were transfected using Lipofectamine™ 3000 Transfection Reagent (Invitrogen, L3000001) for 48 h according to the manufacturer's instructions.

Western blot (WB) analysis

WB was performed as previous described.[19] Briefly, proteins were separated by 10% SDS-PAGE gel and transferred onto PVDF membranes (Tanon, China). After the block with 5% bovine serum albumin for 2 h, membranes were incubated at 4 °C overnight with primary antibodies. Blots were probed with: anti-CXCL11 (ab9955, 0.2 μg/ml), anti-HIF1α (ab51608, 1:200), anti-EGFR (ab52894, 1:1000), anti-phospho-EGFR (ab40815, 1:1000), anti-AKT (ab8805, 1:1000), anti-phospho AKT (ab38449, 1:1000), anti-EGF (ab9695, 0.2 μg/ml), anti-CXCR7 (ab72100, 5 μg/ml), anti-CXCR3 (ab133420, 1/500) and GAPDH (ab8245, 1:10000) (all from Abcam, USA); anti-mTOR (2972, 1:1000), anti-phospho mTOR (5536, 1:1000), anti-Vimentin (5471, 1:1000), anti-Snail (3879, 1:1000), anti-phospho FGFR1 (52928, 1:1000), anti-phospho ALK (14678, 1:1000) and anti-phospho JAK2 (3771, 1:1000) (Cell Signalling Technology, USA); anti-αSMA (BX00010-C3, 1:1000, Biolynx, China); anti-MMP9 (A0289, 1:1000) and anti-GCSF (A6178, 1:1000) (ABclonal, China). Goat anti-rabbit or anti-mouse horseradish peroxidase-conjugated IgG was used as secondary antibody (Santa Cruz Biotechnology). Membranes were visualised using enhanced chemiluminescence detection system (Bio-Rad). Band density was quantified using NIH Image J. Three independent experiments were replicated.

Immunofluorescence (IF)

HUVEC were grown in six-well plates with chamber slides. Specimens were fixed with 4% formaldehyde for 15 min and then rinsed with PBS. Following the block for 60 min, specimens were incubated at 4 °C overnight with primary antibodies. Then, staining was completed as per the manufacturer's instructions.

ELISA

ELISA was performed as per the manufacturer's protocol. The secretive concentration of CXCL11 was investigated using Human Standard ABTS ELISA Development Kit (PeproTech, USA).

Angiogenesis and phospho-RTK antibody array

Human Angiogenesis Antibody Array C1000 and Human RTK Phosphorylation Antibody Array C1 (RayBio® C-Series) were

The role of anlotinib-mediated EGFR blockade in a positive feedback loop...
J Liang et al.

392

employed to analyse the expression of target molecules. These two kits were completed with the same samples. Two groups of CAL-62 were pre-incubated under hypoxia for 24 h. Following the treatment with anlotinib (5 μM) or control medium for another 24 h, cell lysates were harvested and then measured as per the manufacturer's instructions. Raw images were visualised by chemiluminescence detection kit (Millipore, Billerica, MA) and analysed by Image Lab Software (Bio-Rad). Two replicates were included.

PCR array and quantitative real-time PCR
Human angiogenesis PCR array was employed to screen the expression of angiogenetic effectors. Two groups of HUVEC were seeded in a six-well plate at 80% concentration. Then, HUVEC were exposed to the control medium or rhCXCL11 (100 ng/ml) for 2 h, respectively. Total RNA was extracted using TRIzol® Reagent (Ambion). The purity and concentration of RNA were quantified with a UV–Vis spectrophotometer (NanoDrop 1000, USA). cDNA was synthesised with a reverse transcription kit (Toyobo Life Science). Quantitative amplification was achieved using SYBR Green PCR Master Mix (Toyobo Life Science). The used primers are shown in Supplementary Table 2. Relative RNA expression was calculated normalised to GAPDH.

Molecular modelling
3D structure of EGFR was selected from Protein Data Bank (PDB). Following the analysis of resolution power, deleted mutations and binding motif, the crystal structure of EGFR (PDB: 5ugb) was generated as the template for homology modelling using Maestro (Release 2019-2). Besides, the loop motif was further optimised by Refine Structure. EGFR structure was then modified by protonation (pH 7.0), marking bond strength, adding hydrogens and missing side chains using Protein Preparation Wizard in Maestro. Later, the most suitable model was adapted for docking. The structure file of anlotinib was prepared by protonation (pH 7.0 ± 1.5) and bond optimisation in LigPrep. During molecular docking, the receptor-ligand complex was defined as a binding pocket based on the extra precision mode of LigandDocking in Glide. Finally, EGFR-anlotinib binding was further reviewed based on the interacting's rationality using PyMOL.

In vivo Xenograft tumour model, IHC and TUNEL assay
ATC xenograft models in nude mice were established.[20] Four-week-old female BALB/c nude mice were purchased from the Institute of Zoology, Chinese Academy of Sciences of Shanghai. All experiments were performed in accordance with the official recommendations of the Chinese Zoological Society, and animals received humane care according to the criteria outlined in the "Guide for the Care and Use of Laboratory Animals". This animal research was approved by the Ethics Committee of Ruijin Hospital, Shanghai Jiao Tong University School of Medicine.

Suspensions containing CAL-62/EGFR and CAL-62/Vector were subcutaneously injected into the right flank of the nude mice. Mice were divided into three groups, and each group had four mice (group 1: CAL-62/Vector treated with control medium; group 2: CAL-62/Vector treated with anlotinib 60 mg/kg daily; group 3: CAL-62/EGFR treated with anlotinib 60 mg/kg daily). CAL-62 was subcutaneously injected into mice, which were randomly categorised into four different groups, including control, anlotinib, gefitinib and combined treatment with anlotinib and gefitinib daily (each group five mice). The tumour nodules were measured using a Vernier calliper, and the volume was calculated using the formula: $V = \pi/6 \times (W^2 \times L)$. Tumour size was recorded once per week. After ~2 weeks, when the tumours reached ~80 mm³, anlotinib, gefitinib or control medium was administered via oral gavage daily. Mice were euthanised by cervical decapitation after 7 weeks, and tumours were removed, weighed and fixed in formalin. IHC was performed as previously described.[20]

Human breast carcinoma tissue (phospho-EGFR, HIF1α, EGF, Ki67), liver tissue (CXCL11) and tonsil tissue (CD31) were selected as a positive control. Negative control was the paraffin section of ATC xenograft, which were stained without primary antibody, but only secondary antibody. Antibodies included anti-phospho-EGFR (phospho-Y1068, ab40815, 1:250), anti-HIF1α (ab51608, 1:100), anti-CXCL11 (ab9955, 1 μg/ml) and anti-EGF (ab9695, 1 μg/ml, all from Abcam). Moreover, tumour's proliferation and microvascular density were decided by Ki67 (bp6132, 1:300, Biolynx) and CD31 (ab28364, 1:50, Abcam), respectively. IHC images were evaluated by a pathologist. TUNEL assay was performed using In Situ Cell Death Detection Kit, Fluorescein (Roche Applied Science, USA) and nuclei were screened by DAPI.

Statistical analysis
Statistical analyses were processed using SPSS Statistics 24 (IBM, USA) and GraphPad Prism 6. One-way ANOVA and Student's t test were chosen for comparison among groups. Pearson correlation coefficient was used to analyse the correlations. Categorical data were evaluated with the Chi-square test or Fisher's exact test. $P < 0.05$ were considered significant.
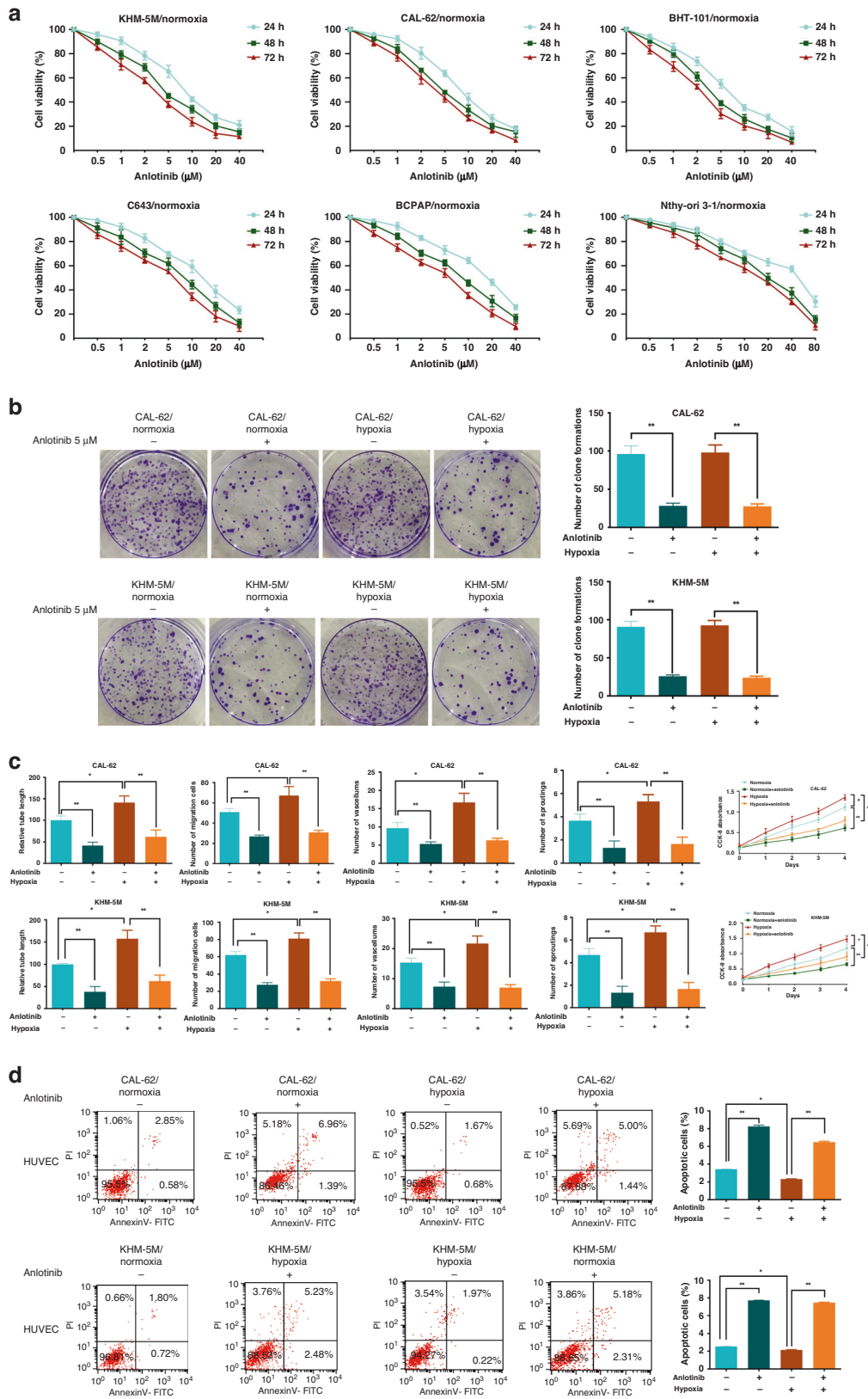
RESULTS
Anlotinib suppresses hypoxia-activated angiogenesis in ATC
The results of the CCK-8 assay indicated that anlotinib dose- and time-dependently inhibited the proliferation of ATC cells under normoxia (Fig. 1a) and hypoxia (Fig. S1A). The 50% inhibitory concentration (IC50) values of anlotinib in ATC cells are listed in Supplementary Table 3. The IC50 at 24 h in Nthy-ori 3-1, a normal thyroid cell line, was 42.85 μM, which was apparently higher than that in ATC cells. Thus, the inhibitory effect of anlotinib on Nthy-ori 3-1 cell is relatively weak. As shown in Fig. 1b, hypoxia had little influence on the colony formation of CAL-62 and KHM-5M cells; however, a substantial decline in the number of colonies after anlotinib treatment was detected under normoxic and hypoxic conditions.

Multiple in vitro assays (tubule formation, 3D sprouting, HUVEC migration and proliferation, apoptosis, and screening of EndMT markers) and in vivo CAM assay were used to evaluate the angiogenetic effects. CAL-62 and KHM-5M cells were treated with 1 μM anlotinib; this concentration is below the IC_{50} value and represses cell growth without conspicuous cytotoxicity. Stronger angiogenic effects, including longer tubule length, the higher number of buddings and CAM vessels were detected under hypoxia; however, anlotinib considerably reduced hypoxia-induced angiogenesis in CAL-62 and KHM-5M cells (Fig. 1c and Fig. S1B, C). The level of new vessel formation is influenced by the changes of migration and number of HUVEC. These two possibilities were investigated using transwell, EndMT, CCK-8 and apoptosis assays. Hypoxia could enhance HUVEC migration and proliferation, and further decrease apoptosis rate; these effects could be reversed upon anlotinib treatment (Fig. 1c, d and Fig. S1C). Similarly, EndMT was promoted under hypoxia because the levels of αSMA, Vimentin and Snail were upregulated. These changes induced by hypoxia were abrogated by anlotinib (Fig. S1D). The same changes of αSMA and Vimentin were confirmed by the IF as well (Fig. S1E). Overall, these in vitro and in vivo findings suggest that anlotinib can inhibit ATC angiogenesis by restraining cell migration, the number of cells under hypoxia with higher efficiency than that observed under normoxia.

CXCL11 mediates anlotinib inhibition of hypoxia-activated angiogenesis
Samples of CAL-62 treated with anlotinib and control medium under hypoxia were investigated by angiogenesis antibody array (Fig. S2A). Importantly, a number of cytokines were down-regulated, including CXCL11, CCL2, MMP9, PDGF-BB, CCL13 and

The role of anlotinib-mediated EGFR blockade in a positive feedback loop...
J Liang et al.

393

CCL7 (Fig. 2a). These results indicated that the anti-angiogenic effect of anlotinib under hypoxia was mediated by a complex mechanism involving numerous genes, especially chemokines. Furthermore, the effects of HIF1α on the transcription activity of angiogenic molecules were also predicted by JASPAR (http://jaspar.genereg.net/). Only CXCL11, MMP9, VEGFR2 and GCSF were downregulated by anlotinib and also induced by HIF1α (Fig. S2B). A series of WB assays were performed to test the expression of

The role of anlotinib-mediated EGFR blockade in a positive feedback loop...
J Liang et al.

394

Fig. 1 Anlotinib suppresses hypoxia-activated angiogenesis in ATC. a ATC cells were treated with a control medium or a series of concentration of anlotinib (0.5, 1, 2, 5, 10, 20, 40 and 80 μM) under normoxia for 24, 48 and 72 h. Cell viability was assessed by CCK-8 assay. **b** Representative images of contact-dependent clone formation and quantification of the clone number in CAL-62 and KHM-5M cells (hypoxia: 2% concentration of O_2; concentration of Anlotinib: 5 μM). **c** Compared with the control groups, the angiogenic abilities including tubule formation, HUVEC migration, 3D sprouting, CAM vessel and HUVEC proliferation were promoted by the supernatants from CAL-62 and KHM-5M cells under hypoxia and repressed by anlotinib treatment. Histograms show the relative tubule length and the numbers of migration cells, sprout buddings and CAM vessels. **d** The apoptotic rate of HUVEC incubated by supernatants collected from CAL-62 and KHM-5M cells treated with anlotinib under hypoxia. All data are obtained from three independent experiments. *$P < 0.05$; **$P < 0.01$.
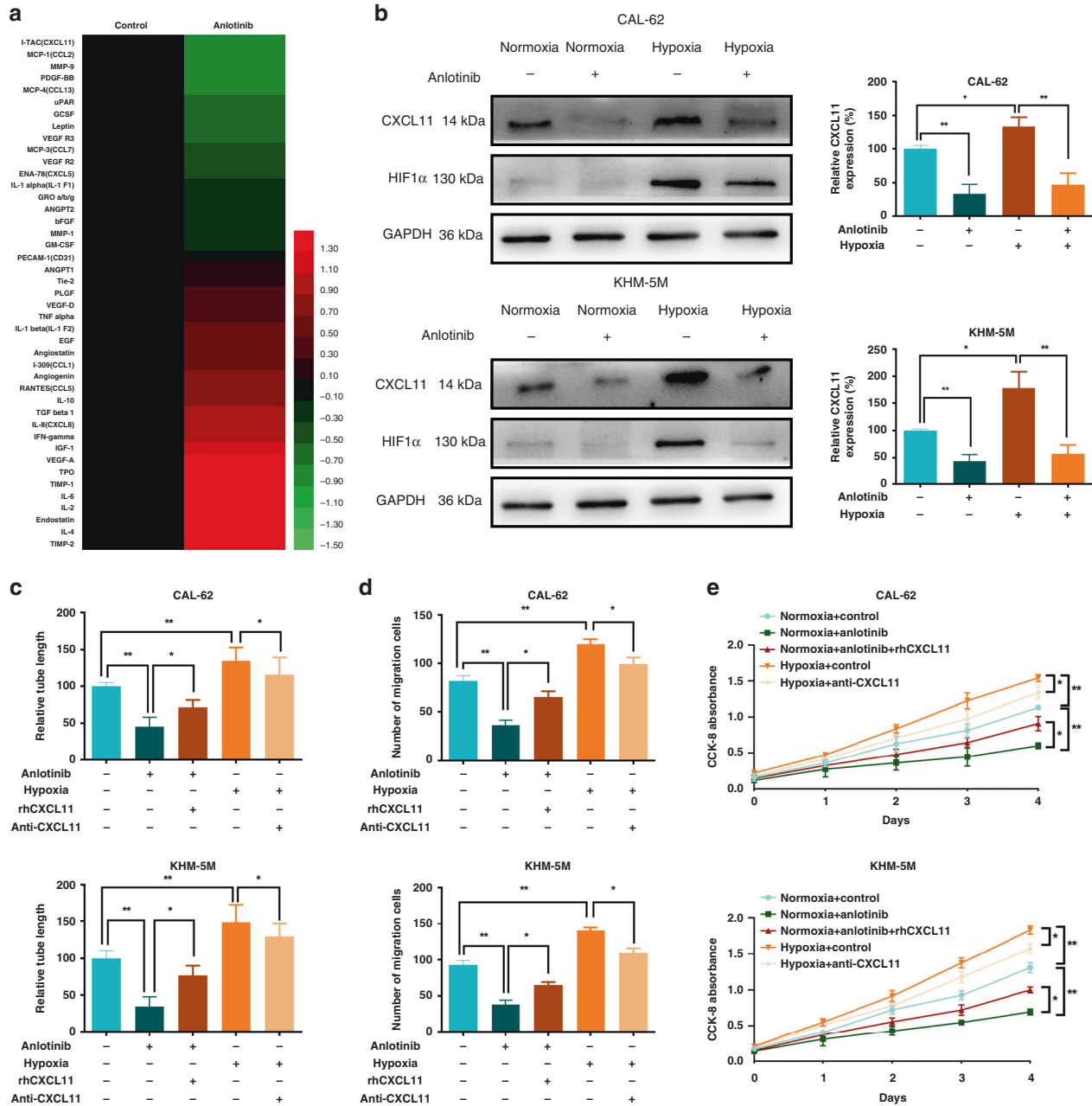
Fig. 2 CXCL11 mediates anlotinib inhibition of hypoxia-activated angiogenesis. a Heatmap of the molecular changes from the angiogenesis antibody array, which was performed under hypoxia (2% concentration of O_2). **b** The CXCL11 production under hypoxia or anlotinib treatment in CAL-62 and KHM-5M cells. **c–e** Addition of rhCXCL11 into the supernatants from CAL-62 and KHM-5M cells treated with anlotinib could reverse anlotinib's anti-angiogenic abilities; adding CXCL11 neutralise antibody into the supernatants from CAL-62 and KHM-5M cells treated with hypoxia could partly attenuate hypoxia-induced angiogenesis. Angiogenic assays included tubule formation (**c**), HUVEC migration (**d**) and HUVEC proliferation (**e**). All data are obtained from three independent experiments. *$P < 0.05$; **$P < 0.01$.

The role of anlotinib-mediated EGFR blockade in a positive feedback loop...
J Liang et al.

395

these four targets (Fig. S2C and Fig. 2b). CXCL11 showed maximal reduction and a high possibility of hypoxia activation. Then, ELISA targeting CXCL11 was performed to confirm the results of the screening array (Fig. S2D). CXCL11 was upregulated under hypoxia, and this effect was significantly decreased after anlotinib exposure in CAL-62 and KHM-5M cells. Consistently, PCR confirmed that anlotinib could downregulate the hypoxia-upregulated levels of CXCL11 (Fig. S2E). Thus, CXCL11 can be regulated at the mRNA and protein levels in ATC cells exposed to anlotinib or hypoxia.

CXCL11 is an important chemokine that influences endothelium during the progression of malignancies.[21] Therefore, we determined whether CXCL11-mediated angiogenesis promoted and repressed by hypoxia and anlotinib, respectively. rhCXCL11 was used to transiently activate CXCL11 expression after anlotinib treatment, and anti-CXCL11 was used to deactivate CXCL11 under hypoxia. Addition of rhCXCL11 to the supernatant of anlotinib-treated CAL-62 and KHM-5M cells enhanced tubule length (Figs. 2c and S2F), HUVEC migrations (Figs. 2d and S2G), HUVEC proliferation (Fig. 2e) and EndMT of HUVEC (Fig. S2H) compared with those in the group treated with anlotinib alone. The addition of anti-CXCL11 to the hypoxia-induced supernatants resulted in a decrease in the tubule length, HUVEC migration and proliferation, and EndMT (Fig. 2c–e and Fig. S2F–H). Overall, these results suggest an important role of CXCL11 in the anti- and proangiogenic effects of anlotinib and hypoxia, respectively.

CXCL11 promotes angiogenesis in ATC
To determine the expression pattern of CXCL11 in ATC tissues, IHC of CXCL11 was performed in a cohort of 50 ATC tumour and peritumour tissues (Fig. S3A). The average expression score of CXCL11 in the tumour was significantly higher than that in the peritumour (Fig. 3a). To evaluate the function of CXCL11 at the cellular level, the basal production of CXCL11 in ATC cells was assayed by WB (Fig. S3B). Consistent with the pattern detected at the tissue level, ATC cells had higher CXCL11 expression compared with that in Nthy-ori 3-1 cells.

To explore the proangiogenic effects of CXCL11 in ATC, we initially determined that rhCXCL11 could promote maximal angiogenesis at a concentration of 100 ng/ml in 2 h (Fig. 3b and Fig. S3C). Then, CXCL11 was knocked down and overexpressed in CAL-62 and KHM-5M cells (Fig. S3D). Supernatants from CAL-62/siCXCL11 and KHM-5M/siCXCL11 cells induced significantly decreased tubule length, HUVEC migration and proliferation, and EndMT ability (Fig. 3c and Fig. S3E–G). In contrast, overexpression of CXCL11 improved angiogenic activity (Fig. 3d and Fig. S3H–J). Notably, CXCL11-regulated angiogenic activities were reversed by cotreatment with rhCXCL11 or anti-CXCL11, respectively. These results convincingly validate the proangiogenic properties of CXCL11 in ATC.

CXCL11 activates endothelial cells by promoting EGF expression
Chemokine-mediated angiogenesis commonly involves downstream proangiogenic cytokines. A PCR array was used to identify the downstream effector of CXCL11. As shown in Fig. 3e, the levels of 11 factors were decreased; however, the levels of the other eleven angiogenic genes were increased. CXCL5, LEP, EGF, TPO and IFNG demonstrated the top increase. Among them, the results of PCRs indicated a most considerable upregulation of EGF in HUVEC treated with rhCXCL11 (Fig. S3K). Together with the promising capacity of pro-angiogenesis of EGF, EGF might be the downstream target of CXCL11.

CXCR7 and CXCR3 are the known CXCL11 receptors.[22] At the mRNA level, upregulation of EGF was blocked by silencing CXCR7 in HUVEC treated with rhCXCL11; however, this blockade was not detected when CXCR3 was knocked down (Fig. S3L, M). A similar trend was detected by WB (Fig. 3f). In addition, CXCL11 content was increased in WB but not in PCR after rhCXCL11 incubation

(Fig. 3f and Fig. S3N). Subsequently, HUVEC were incubated with the supernatants from CAL-62/CXCL11 and KHM-5M/CXCL11 cells and the corresponding control cells. WB targeting EGF validated CXCL11-mediated EGF activation in a CXCR7 dependent manner (Fig. 3g, h).

Since CXCR7 knockdown is known to induce apoptosis of endothelial cells,[23] apoptosis was assayed to validate the effect of CXCL11-CXCR7 signalling on HUVEC. As shown in Fig. S3O, depletion of CXCR7 could increase apoptosis of endothelial cells. Furthermore, CXCL11 and EGFR signalling barely influenced the CXCR7 production in HUVEC (Fig. S3P). Furthermore, high expression of CXCR7 was not detected in ATC cells (Fig. S3Q).

The effect of EGFR on endothelium was investigated in Fig. S3R. Upon rhEGF treatment (10 nmol/L for 5 min[24]), siEGFR in HUVEC significantly decreased the levels of p-EGFR, αSMA and Vimentin. Thus, EGF influenced endothelium in an EGFR-dependent manner indicating the presence of the CXCL11-CXCR7-EGF-EGFR regulatory axis in ATC.

EGFR upregulates CXCL11 in a positive feedback loop in ATC
ATC tissue array previously used to investigate CXCL11 was used to perform IHC of p-EGFR (Fig. S4A). IHC score of p-EGFR was significantly higher in tumour than that in peritumour (Fig. 4a). Importantly, a strong positive correlation between the CXCL11 and p-EGFR levels was detected in ATC tumour ($P = 0.0152$, $r = 0.4797$, Fig. 4b), but not in peritumour (Fig. 4c).

Considering the correlation between CXCL11 and p-EGFR, we hypothesised that a regulatory axis involves EGFR and CXCL11 in ATC. To verify this hypothesis, the basal expression of p-EGFR in ATC cells was evaluated. Higher expression of p-EGFR was detected in ATC cells compared with that in Nthy-ori 3-1 cells (Fig. S4B). This trend was consistent with the pattern detected in the case of CXCL11. Then, the expression levels of CXCL11 and the EGFR-AKT-mTOR pathway were assayed after EGFR knockdown in CAL-62 and KHM-5M cells. The levels of CXCL11 and the signalling molecules were significantly decreased (Fig. 4d, e). EGFR overexpression and rhEGF stimulation in CAL-62 and KHM-5M cells could upregulate the AKT-mTOR cascade and CXCL11 (Fig. S4C, D). Thus, these results suggest the presence of a positive CXCL11-EGF-EGFR feedback loop, which bridge the crosstalk between cancer and vascular cells. The Akt-mTOR pathway is involved in the regulation of hypoxia and anlotinib in ATC.

CXCL11 restoration in CAL-62/siEGFR or KHM-5M/siEGFR cells partly reversed a reduction in angiogenic activities (Fig. 4f and Fig. S4E, F). These assays were replicated in ATC cells ectopically overexpressing EGFR, and angiogenesis was attenuated in the presence of anti-CXCL11 (Fig. 4g and Fig. S4G, H). Thus, EGFR enhances angiogenesis partly in a CXCL11-dependent manner in ATC.

Anlotinib directly targets EGFR kinase
Anlotinib is a phospho-RTK inhibitor; hence, the phospho-RTK antibody array was used to identify a potential target of anlotinib. Four targets (p-EGFR, p-ALK, p-JAK2 and p-FGFR1) were significantly downregulated by anlotinib (Fig. 5a and Fig. S5A). The results of WB verified a decrease in p-EGFR in all cell lines after anlotinib treatment (Fig. S5B). Moreover, EGFR-AKT signalling was increased under hypoxia in CAL-62 and KHM-5M cells and was decreased by anlotinib treatment (Fig. 5b). To demonstrate that EGFR is required for anlotinib-mediated CXCL11 reduction, overexpression of EGFR was performed when treatment with anlotinib. Consequently, the decline in CXCL11 was reversed due to the restoration of EGFR in CAL-62 and KHM-5M cells, and anlotinib could more efficiently inhibit EGFR-AKT signalling, and also CXCL11 production in EGFR-positive cells (Fig. 5c).

A molecular docking model was used to confirm the direct association between EGFR and anlotinib. As shown in Figs. 5d and S5C, anlotinib occupies the ATP-binding pocket of EGFR. In detail,

The role of anlotinib-mediated EGFR blockade in a positive feedback loop…
J Liang et al.

396
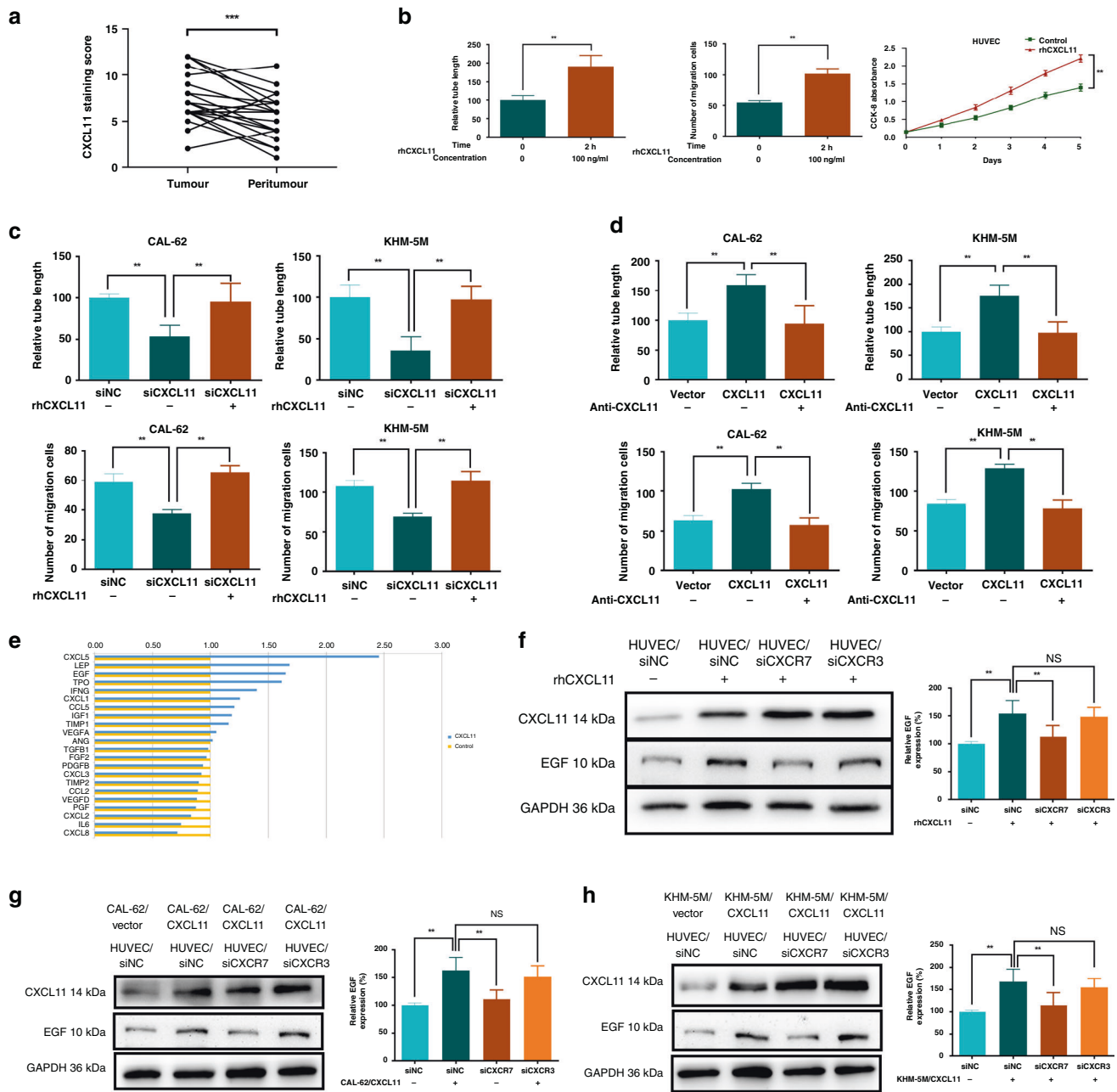
Fig. 3 CXCL11 promotes angiogenesis by promoting EGF expression in ATC. a The average expression score of CXCL11 in the tumour was higher than that in matched peritumour from ATC tissue microarray. **b** rhCXCL11 (100 ng/ml for 2 h) could improve the abilities of tubule formation, migration and proliferation of HUVEC. **c** Supernatants from CXCL11 knockdown ATC cells could decrease the tubule formation and migration of HUVEC. **d** Supernatants from CXCL11 overexpression ATC cells could increase the tubule formation and migration of HUVEC. **e** Quantification of up- and downregulated angiogenetic genes by PCR array with HUVEC treated by rhCXCL11 (100 ng/ml for 2 h) against negative control. **f** Expression of EGF was detected when HUVEC treated with rhCXCL11 under CXCR3 or CXCR7 knockdown. **g, h** HUVEC was cultured with supernatants from CAL-62 and KHM-5M cells overexpressing CXCL11. All data are obtained from three independent experiments. *$P < 0.05$; **$P < 0.01$; ***$P < 0.001$.

anlotinib interacts with EGFR by forming hydrogen bonds with Met793, Pro794, Asn842 and Asp855. Moreover, a cation–π interaction between Lys52 of EGFR and the benzene ring of anlotinib enhances the strength of the binding. Therefore, EGFR is the inhibitory target of anlotinib in ATC. From Fig. S4B, Nthy-ori 3-1 cells retain the low expression of p-EGFR. This may be the reason why the inhibitory effect of anlotinib that acts on EGFR is relatively weak in Nthy-ori 3-1 cells.

In addition, anlotinib repressed the viability of endothelial cells activated by EGF (Fig. 5e and Fig. S5D). Angiogenesis was

substantially inhibited. These results suggest that anlotinib can repress ATC angiogenesis *via* two mechanisms, including simultaneous direct targeting of EGFR on cancer and endothelial cells.

Anlotinib delays tumorigenesis in vivo
Considering the in vitro findings, a xenograft model was used to validate the inhibitory effect of anlotinib on ATC in vivo. Comparison with the control group indicated that treatment with anlotinib decreased tumour weight and volume. EGFR over-expression partly suppressed the inhibitory effect of anlotinib

The role of anlotinib-mediated EGFR blockade in a positive feedback loop...
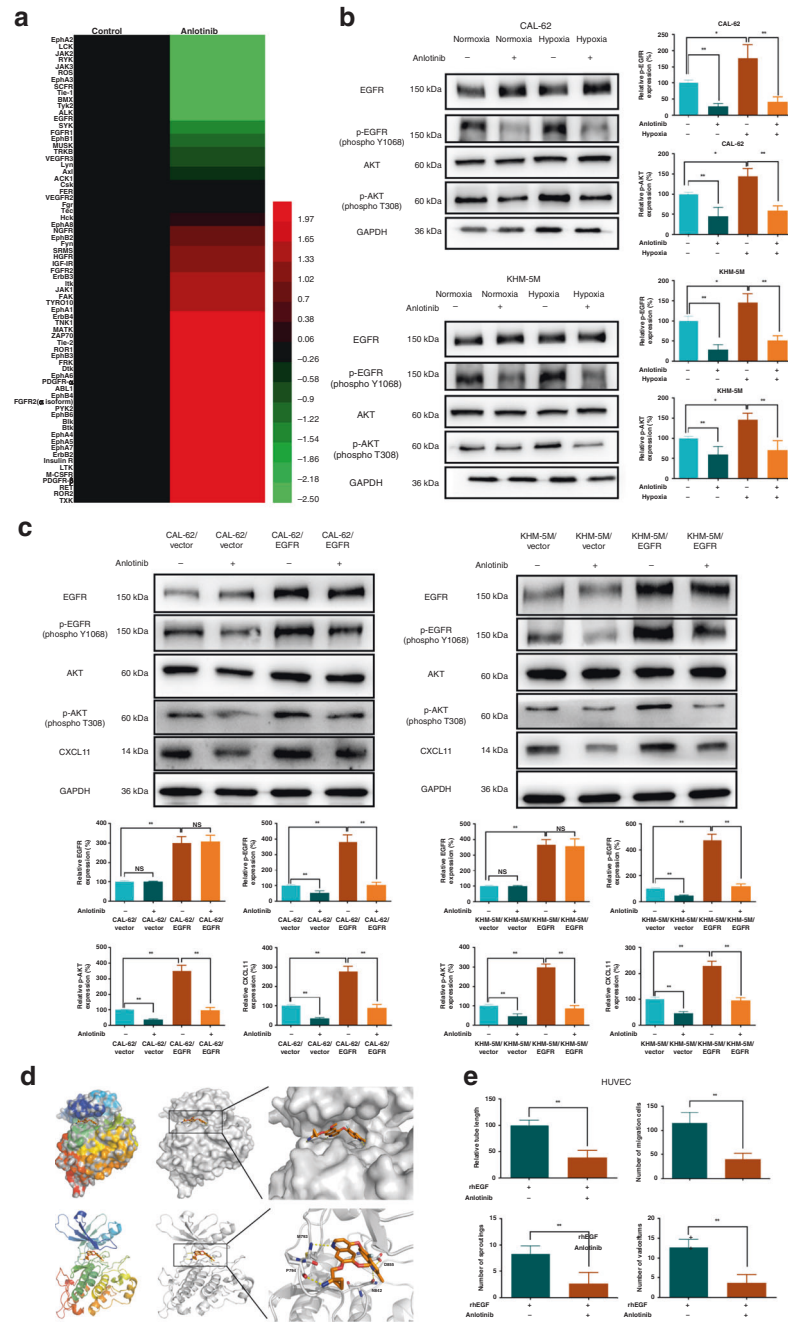J Liang et al.

397

(Fig. 6a–c). Tumourigenic and angiogenic markers were assayed by IHC. Comparison with the control group indicated that the tumours in the anlotinib group had lower expression levels of Ki67 and CD31, and signalling molecules (p-EGFR, HIF1α, CXCL11 and EGF) (Fig. 6d, e). An enhanced TUNEL staining was observed in the anlotinib group (Fig. 6d). Changes in these markers were partly
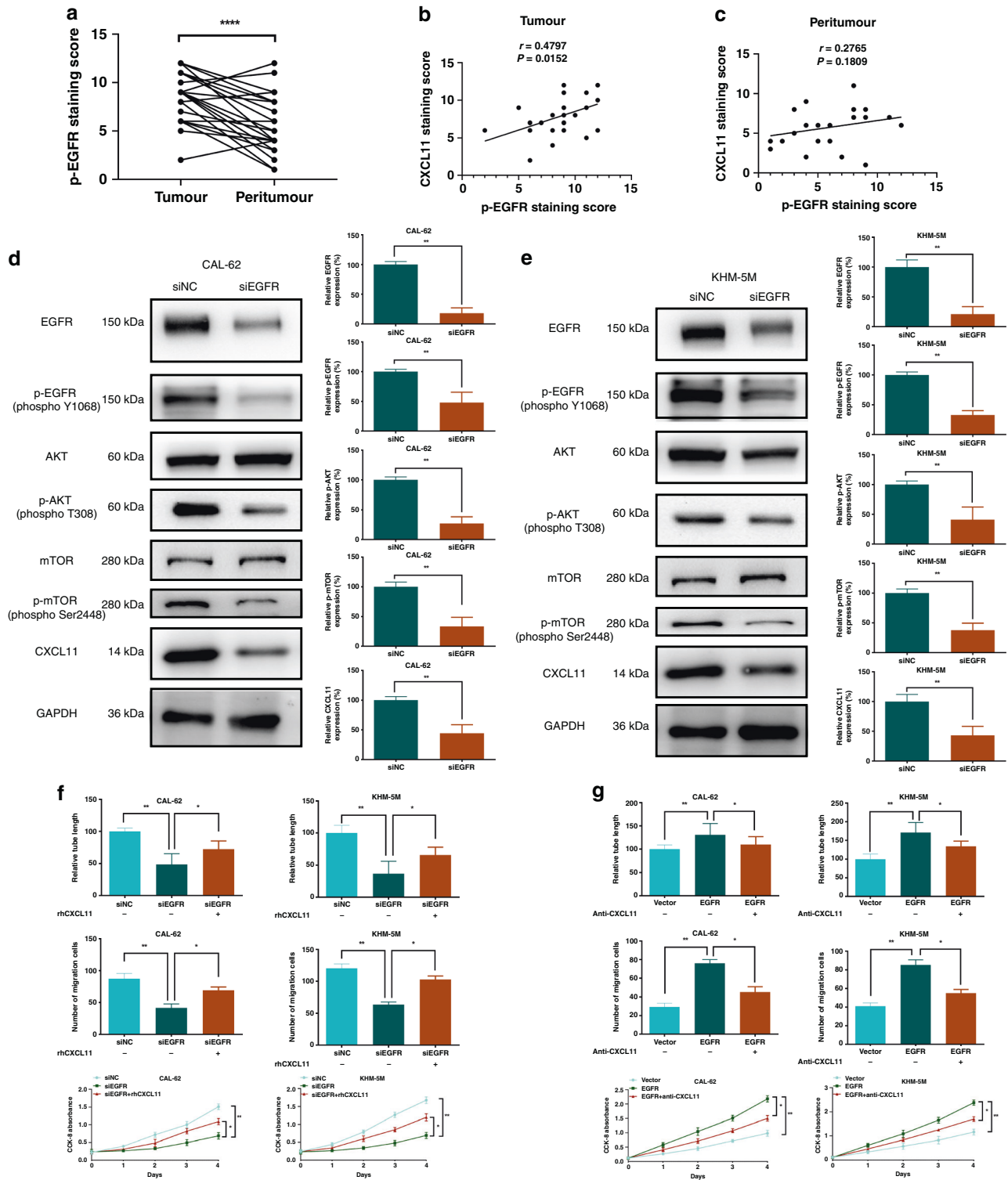
Fig. 4 **EGFR upregulates CXCL11 in a positive feedback loop in ATC. a** The average expression score of phospho-EGFR in tumour was higher than that in matched peritumour from ATC tissue microarray. **b**, **c** The strong positive correlation between CXCL11 and phospho-EGFR was found in ATC tumour, but not in peritumour. **d**, **e** CXCL11 production and AKT-mTOR signalling were influenced by EGFR knockdown in CAL-62 and KHM-5M cells. **f** Supernatants from CAL-62/siEGFR or KHM-5M/siEGFR cells with CXCL11 restoration could partly reverse the reduction of tube formation, cell migration and proliferation of HUVEC. **g** Supernatants from EGFR overexpression cells with CXCL11 depletion could attenuate the EGFR-activated tube formation, cell migration and proliferation of HUVEC in CAL-62 and KHM-5M. All data are obtained from three independent experiments. *$P < 0.05$; **$P < 0.01$; ****$P < 0.0001$.

The role of anlotinib-mediated EGFR blockade in a positive feedback loop…
J Liang et al.

398

Fig. 5 Anlotinib directly targets EGFR kinase. a Heatmap of the molecular changes from the phospho-RTK antibody array, which was completed by using the same samples like that in the angiogenesis antibody array. **b** Expression level of p-EGFR and p-AKT was examined when CAL-62 and KHM-5M cells were treated by anlotinib under normoxia and hypoxia. **c** CXCL11 production was increased in EGFR overexpression cells, and anlotinib could more efficiently inhibit the EGFR-AKT signalling and CXCL11 production in CAL-62/EGFR and KHM-5M/EGFR cells compared with their Vector controls. **d** Cartoon representations of the anlotinib's binding pocket in EGFR in visualised models of molecular docking. Residues of Met793, Pro794, Asn842 and Asp855 of EGFR were predicted to interact with anlotinib by hydrogen bonds. The ligands are shown in orange sticks, while proteins are depicted in cartoon representation with key residues. Hydrogen bonds are shown as yellow dashed lines. **e** Anlotinib repressed angiogenetic abilities by directly inhibiting HUVEC, including tubule formation, migration, 3D buddings and CAM vessels. All data are obtained from three independent experiments. *$P < 0.05$; **$P < 0.01$.

abrogated by EGFR overexpression. These in vivo data indicated that anti-angiogenic activity of anlotinib is mainly mediated by EGFR.

EGFR is a classical druggable target, and numerous EGFR inhibitors have been developed, including gefitinib.[25–27] Therefore, we investigated the combined effects of anlotinib and gefitinib in vivo. Mice with ATC tumours were exposed to anlotinib, gefitinib or their combination. Gefitinib suppressed the growth of ATC; however, its inhibitory effect was relatively weaker than that detected in the anlotinib group. Moreover, a combination of gefitinib with anlotinib did not significantly increase the inhibitory activity of anlotinib compared with that in mice treated with anlotinib alone (Fig. 6f, g). This in vivo result indicates that anlotinib may have superior anti-oncogenic effects in ATC.

The role of anlotinib-mediated EGFR blockade in a positive feedback loop...
J Liang et al.

399
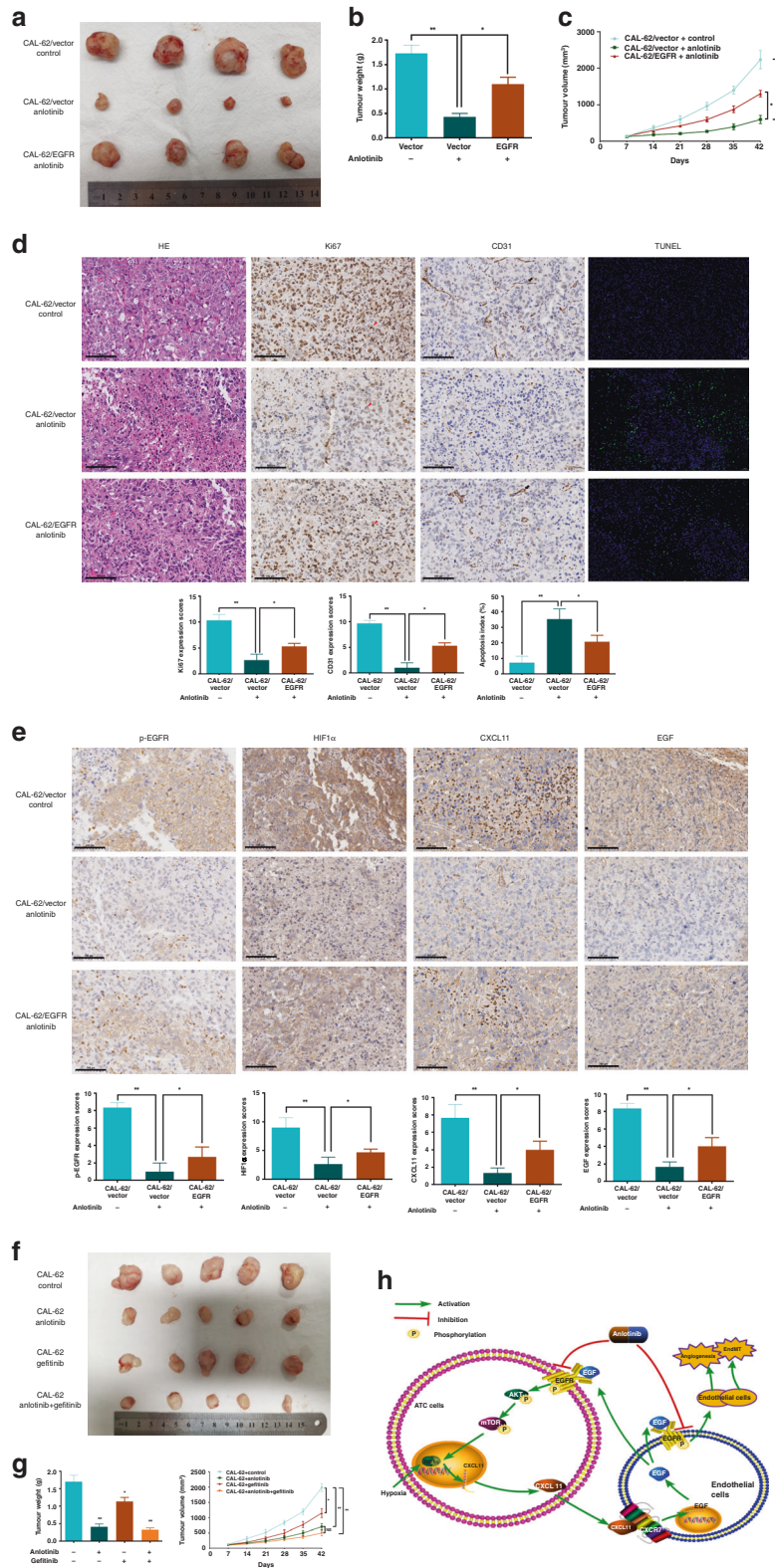
Fig. 6 Anlotinib delays tumorigenesis in vivo. a Tumours of xenograft mice injected with CAL-62/Vector and CAL-62/EGFR. The mice were given by gavage with anlotinib (60 mg/kg) or control medium daily. **b** Quantification of tumour weights after mice sacrifice. **c** Tumour volumes were measured every week. **d**, **e** Images and quantifications of TUNEL assay and IHC staining of Ki67, CD31, p-EGFR (phospho-Y1068), HIF1α, CXCL11 and EGF. Red arrowhead means tumour cells, and black arrow means endothelial cells. **f** Xenograft models were generated by injecting CAL-62. Four groups of mice were treated with control medium, anlotinib, gefitinib and a combination of two agents. **g** Quantification of tumour volumes and weights of the four groups. **h** The schematic of anlotinib blocking cancer–endothelium crosstalk in ATC. Anlotinib inhibited hypoxia-induced positive CXCL11-EGF-EGFR feedback loop by direct binding to EGFR on both cancer and vascular cells. *P < 0.05; **P < 0.01.

The role of anlotinib-mediated EGFR blockade in a positive feedback loop...
J Liang et al.

400

DISCUSSION

Cytotoxicity is considered the main effect of anlotinib; however, anti-angiogenic activity is also important.[28] In this study, we confirmed that hypoxia promotes angiogenesis in ATC and that anlotinib inhibits hypoxia-induced angiogenesis more efficiently under hypoxia than under normoxia. Direct binding of anlotinib to EGFR repressed hypoxia-activated positive CXCL11-EGF-EGFR feedback loop, which bridge the interactions between ATC and endothelial cells. Therefore, the novel mechanism in Fig. 6h demonstrated the anti-angiogenic effects of anlotinib on ATC, which is in different from previous interpretations.[29,30]

Under hypoxia, HIF1α increases the release of proangiogenic factors, including VEGF, EGF and FGF, and CCL- and CXCL-chemokines.[31,32] Some reports suggest that CXCL11 is one of the important factors that regulate the tumour microenvironment under hypoxia.[33] However, another study reports that CXCL11 level is not influenced by low oxygen.[34] Our study demonstrated a constitutive release of CXCL11 under hypoxia in ATC. This discrepancy may result from distinctive signatures and functions of CXCL11 in different tumours.

The angiogenic potential of CXCL11 is neglected in some reports;[35] however, there is no general consensus about the angiogenic activity of CXCL11.[22,36] Our experimental data demonstrated the proangiogenic activity of CXCL11 in ATC. CXCL11 receptors, CXCR3 and CXCR7, have different effects on the biological activities of CXCL11.[22,37] Unlike dual effects of CXCR3 on angiogenesis in other cancers,[38] CXCR3 was not involved in CXCL11-mediated angiogenesis in ATC. However, CXCR7 is able to enhance angiogenesis.[39] Knockdown of CXCR7 attenuated CXCL11-mediated angiogenesis. Our data indicate that CXCL11-induced angiogenesis predominantly depends on CXCR7 signalling in ATC.

CXCR7 can promote cell proliferation by coordinating the EGFR signalling.[40] However, in addition to physical association, the CXCL11 binding to and activation of CXCR7 regulates EGF production in ATC. Consequently, CXCR7 regulates EGFR activity by influencing the EGF-EGFR pathway. Thus, our study proposes a novel mechanism of action of CXCL11-CXCR7 that involves the EGF-EGFR signalling.

EGFR plays an important role in ATC progression,[41–44] and VEGF is the principal mediator of EGFR-induced angiogenesis.[45,46] Interestingly, EGFR influences CXCL11 production, and EGFR-mediated angiogenesis is dependent on the involvement of CXCL11, based on the results of the present study. Therefore, CXCL11 is an upstream promoter of the EGF-EGFR signalling and a downstream effector of EGFR activation. This newly identified positive intercellular crosstalk between cancer and vascular cells represents a novel mechanism of angiogenesis in ATC. Overall, our study defined a positive feedback loop of the CXCL11-EGF-EGFR signalling, which is considerably activated by hypoxia in ATC.

Anlotinib is a broad-spectrum anti-oncogenic agent that conventionally targets VEGFR, FGFR and PDGFR.[47,48] Recent studies on the possible mechanisms of action of anlotinib identified an increasing number of unconventional pharmacologic targets, such as MET.[49] and GINS1.[50] Our experimental data indicates that EGFR is a novel target of anlotinib; this study is the first to confirm this phenomenon. Phospho-EGFR, rather than the known targets, was downregulated in ATC cells treated with anlotinib. In addition, anlotinib blocked intercellular crosstalk via a dual mechanism by simultaneous inhibitory effects on cancer cells and endothelium. Thus, the inhibitory potential of anlotinib can be expanded and may help to develop new therapeutic strategies in ATC.

In summary, this study is the first to demonstrate the effects of anlotinib on the regulatory network of cellular interactions between ATC and endothelial cells. The positive CXCL11-EGF-E-GFR feedback loop provides mechanistic insight into the cancer–endothelium crosstalk under hypoxia, and EGFR is a newly identified target. Our preclinical findings can be used as a proof-of-concept demonstrating the therapeutic effects of anlotinib in ATC.

AUTHOR CONTRIBUTIONS

W.Q., X.C., B.S. and J.Y. designed the study. W.C. and J.K. analysed the data and revised the manuscript. J.L. wrote the manuscript. J.L. and Z.J. performed most of the experiments. H.F., Q.Z., Z.Y. and L.Z. performed the experiments. All of the authors discussed the results, reviewed and approved the final manuscript.

REFERENCES

1. Siegel, R. L., Miller, K. D. & Jemal, A. Cancer statistics, 2020. *CA: A Cancer J. Clin.* **70**, 7–30 (2020).
2. Xu, B. & Ghossein, R. Genomic landscape of poorly differentiated and anaplastic thyroid carcinoma. *Endocr. Pathol.* **27**, 205–212 (2016).
3. Molinaro, E., Romei, C., Biagini, A., Sabini, E., Agate, L., Mazzeo, S. et al. Anaplastic thyroid carcinoma: from clinicopathology to genetics and advanced therapies. *Nat. Rev. Endocrinol.* **13**, 644–660 (2017).
4. Wu, H., Sun, Y., Ye, H., Yang, S., Lee, S. L. & de las Morenas, A. Anaplastic thyroid cancer: outcome and the mutation/expression profiles of potential targets. *Pathol. Oncol. Res.* **21**, 695–701 (2015).
5. Saini, S., Tulla, K., Maker, A. V., Burman, K. D. & Prabhakar, B. S. Therapeutic advances in anaplastic thyroid cancer: a current perspective. *Mol. Cancer* **17**, 154 (2018).
6. Smallridge, R. C. & Copland, J. A. Anaplastic thyroid carcinoma: pathogenesis and emerging therapies. *Clin. Oncol.* **22**, 486–497 (2010).
7. Ema, M., Taya, S., Yokotani, N., Sogawa, K., Matsuda, Y. & Fujii-Kuriyama, Y. A novel bHLH-PAS factor with close sequence similarity to hypoxia-inducible factor 1α regulates the VEGF expression and is potentially involved in lung and vascular development. *Proc. Natl Acad. Sci. USA* **94**, 4273–4278 (1997).
8. Niu, Y., Bao, L., Chen, Y., Wang, C., Luo, M., Zhang, B. et al. HIF2-induced long noncoding RNA RAB11B-AS1 promotes hypoxia-mediated angiogenesis and breast cancer metastasis. *Cancer Res.* **80**, 964 (2020).
9. Hogenesch, J. B., Gu, Y. Z., Jain, S. & Bradfield, C. A. The basic-helix-loop-helix-PAS orphan MOP3 forms transcriptionally active complexes with circadian and hypoxia factors. *Proc. Natl Acad. Sci. USA* **95**, 5474–5479 (1998).
10. Schito, L. & Semenza, G. L. Hypoxia-inducible factors: master regulators of cancer progression. *Trends Cancer* **2**, 758–770 (2016).

The role of anlotinib-mediated EGFR blockade in a positive feedback loop…
J Liang et al.

401

11. Maxwell, P. H., Wiesener, M. S., Chang, G. W., Clifford, S. C., Vaux, E. C., Cockman, M. E. et al. The tumour suppressor protein VHL targets hypoxia-inducible factors for oxygen-dependent proteolysis. *Nature* **399**, 271–275 (1999).

12. Wang, G. L., Jiang, B. H., Rue, E. A. & Semenza, G. L. Hypoxia-inducible factor 1 is a basic-helix-loop-helix-PAS heterodimer regulated by cellular O2 tension. *Proc. Natl Acad. Sci. USA* **92**, 5510–5514 (1995).

13. Rey, S., Schito, L., Wouters, B. G., Eliasof, S. & Kerbel, R. S. Targeting hypoxia-inducible factors for antiangiogenic cancer therapy. *Trends Cancer* **3**, 529–541 (2017).

14. Ha, H. T., Lee, J. S., Urba, S., Koenig, R. J., Sisson, J., Giordano, T. et al. A Phase II study of imatinib in patients with advanced anaplastic thyroid cancer. *Thyroid* **20**, 975–980 (2010).

15. Bueno, M. J., Mouron, S. & Quintela-Fandino, M. Personalising and targeting antiangiogenic resistance: a complex and multifactorial approach. *Br. J. Cancer* **116**, 1119–1125 (2017).

16. Sun, Y., Niu, W., Du, F., Du, C., Li, S., Wang, J., Li, L., Wang, F. et al. Safety, pharmacokinetics, and antitumor properties of anlotinib, an oral multi-target tyrosine kinase inhibitor, in patients with advanced refractory solid tumors. *J. Hematol. Oncol.* **9**, 105 (2016).

17. Cheng, X., Jin, Z., Ji, X., Shen, X., Feng, H., Morgenlander, W. et al. ETS variant 5 promotes colorectal cancer angiogenesis by targeting platelet-derived growth factor BB. *Int. J. Cancer* **145**, 179–191 (2019).

18. Nowak-Sliwinska, P., Alitalo, K., Allen, E., Anisimov, A., Aplin, A. C., Auerbach, R. et al. Consensus guidelines for the use and interpretation of angiogenesis assays. *Angiogenesis* **21**, 425–532 (2018).

19. Fu, Z., Cheng, X., Kuang, J., Feng, H., Chen, L., Liang, J. et al. CQ sensitizes human pancreatic cancer cells to gemcitabine through the lysosomal apoptotic pathway via reactive oxygen species. *Mol. Oncol.* **12**, 529–544 (2018).

20. Feng, H., Cheng, X. I., Kuang, J., Chen, L., Yuen, S., Shi, M. et al. Apatinib-induced protective autophagy and apoptosis through the AKT-mTOR pathway in anaplastic thyroid cancer. *Cell Death Dis.* **9**, 1030 (2018).

21. Koo, Y. J., Kim, T. J., Min, K. J., So, K. A., Jung, U. S. & Hong, J. H. CXCL11 mediates TWIST1-induced angiogenesis in epithelial ovarian cancer. *Tumour Biol.* **39**, 1010428317706226 (2017).

22. Puchert, M., Obst, J., Koch, C., Zieger, K. & Engele, J. CXCL11 promotes tumor progression by the biased use of the chemokine receptors CXCR3 and CXCR7. *Cytokine* **125**, 154809 (2020).

23. Shen, M., Feng, Y., Wang, J., Yuan, Y. & Yuan, F. CXCR7 inhibits fibrosis via Wnt/β-catenin pathways during the process of angiogenesis in human umbilical vein endothelial cells. *Biomed. Res. Int.* **2020**, 1216926 (2020).

24. Liu, Y., Calmel, C., Desbois-Mouthon, C., Sobczak-Thépot, J., Karaiskou, A. & Praz, F. Regulation of the EGFR/ErbB signalling by clathrin in response to various ligands in hepatocellular carcinoma cell lines. *J. Cell Mol. Med.* **24**, 8091–8102 (2020).

25. Ensinger, C., Spizzo, G., Moser, P., Tschoerner, I., Prommegger, R., Gabriel, M. et al. Epidermal growth factor receptor as a novel therapeutic target in anaplastic thyroid carcinomas. *Ann. N. Y. Acad. Sci.* **1030**, 69–77 (2005).

26. Huang, L. C., Tam, K. W., Liu, W. N., Lin, C. Y., Hsu, K. W., Hsieh, W. S. et al. CRISPR/Cas9 genome editing of epidermal growth factor receptor sufficiently abolished oncogenicity in anaplastic thyroid cancer. *Dis. Markers* **2018**, 1–14 (2018).

27. Lopez, J. P., Wang-Rodriguez, J., Chang, C., Chen, J. S., Pardo, F. S., Aguilera, J. et al. Gefitinib inhibition of drug resistance to doxorubicin by inactivating ABCG2 in thyroid cancer cell lines. *Arch. Otolaryngol. Head Neck Surg.* **133**, 1022–1027 (2007).

28. Liang, L., Hui, K., Hu, C., Wen, Y., Yang, S., Zhu, P. et al. Autophagy inhibition potentiates the anti-angiogenic property of multikinase inhibitor anlotinib through JAK2/STAT3/VEGFA signaling in non-small cell lung cancer cells. *J. Exp. Clin. Cancer Res.* **38**, 71 (2019).

29. Lu, J., Zhong, H., Chu, T., Zhang, X., Li, R., Sun, J. et al. Role of anlotinib-induced CCL2 decrease in anti-angiogenesis and response prediction for non-small cell lung cancer therapy. *Eur. Respir. J.* **53**, 1801562 (2019).

30. Ruan, X., Shi, X., Dong, Q., Yu, Y., Hou, X., Song, X. et al. Antitumor effects of anlotinib in thyroid cancer. *Endocr. Relat. Cancer* **26**, 153–164 (2019).

31. Majmundar, A. J., Wong, W. J. & Simon, M. C. Hypoxia-inducible factors and the response to hypoxic stress. *Mol. Cell* **40**, 294–309 (2010).

32. Semenza, G. L., Nejfelt, M. K., Chi, S. M. & Antonarakis, S. E. Hypoxia-inducible nuclear factors bind to an enhancer element located 3' to the human erythropoietin gene. *Proc. Natl Acad. Sci. USA* **88**, 5680–5684 (1991).

33. Singh, A. K., Arya, R. K., Trivedi, A. K., Sanyal, S., Baral, R., Dormond, O. et al. Chemokine receptor trio: CXCR3, CXCR4 and CXCR7 crosstalk via CXCL11 and CXCL12. *Cytokine Growth Factor Rev.* **24**, 41 (2013).

34. Hensbergen, P. J., Wijnands, P. G. B., Schreurs, M. W., Scheper, R. J., Willemze, R. & Tensen, C. P. The CXCR3 targeting chemokine CXCL11 has potent antitumor activity in vivo involving attraction of CD8+ T lymphocytes but not inhibition of angiogenesis. *J. Immunother.* **28**, 343–351 (2005).

35. Wang, P., Yang, X., Xu, W., Li, K., Chu, Y. & Xiong, S. Integrating individual functional moieties of CXCL10 and CXCL11 into a novel chimeric chemokine leads to synergistic antitumor effects: a strategy for chemokine-based multi-target-directed cancer therapy. *Cancer Immunol. Immunother.* **59**, 1715–1726 (2010).

36. Rupertus, K., Sinistra, J., Scheuer, C., Nickels, R. M., Schilling, M. K., Menger, M. D. et al. Interaction of the chemokines I-TAC (CXCL11) and SDF-1 (CXCL12) in the regulation of tumor angiogenesis of colorectal cancer. *Clin. Exp. Metastasis* **31**, 447–459 (2014).

37. Werner, T. A., Forster, C. M., Dizdar, L., Verde, P. E., Raba, K., Schott, M. et al. CXCR4/CXCR7/CXCL12 axis promotes an invasive phenotype in medullary thyroid carcinoma. *Br. J. Cancer* **117**, 1837–1845 (2017).

38. Billottet, C., Quemener, C. & Bikfalvi, A. CXCR3, a double-edged sword in tumor progression and angiogenesis. *Biochimica et. Biophysica Acta* **1836**, 287–295 (2013).

39. Miao, Z., Luker, K. E., Summers, B. C., Berahovich, R., Bhojani, M. S., Rehemtulla, A. et al. CXCR7 (RDC1) promotes breast and lung tumor growth in vivo and is expressed on tumor-associated vasculature. *Proc. Natl Acad. Sci. USA* **104**, 15735 (2007).

40. Singh, R. K. & Lokeshwar, B. L. The IL-8-regulated chemokine receptor CXCR7 stimulates EGFR signaling to promote prostate cancer growth. *Cancer Res.* **71**, 3268–3277 (2011).

41. Dai, Y. J., Qiu, Y. B., Jiang, R., Xu, M., Zhao, L., Chen, G. G. et al. Concomitant high expression of ERα36, EGFR and HER2 is associated with aggressive behaviors of papillary thyroid carcinomas. *Sci. Rep.* **7**, 12279 (2017).

42. Zhao, L., Zhu, X. Y., Jiang, R., Xu, M., Wang, N., Chen, G. G. et al. Role of GPER1, EGFR and CXCR1 in differentiating between malignant follicular thyroid carcinoma and benign follicular thyroid adenoma. *Int. J. Clin. Exp. Pathol.* **8**, 11236–11247 (2015).

43. Keller, S. & Schmidt, M. H. EGFR and EGFRvIII promote angiogenesis and cell invasion in glioblastoma: combination therapies for an effective treatment. *Int. J. Mol. Sci.* **18**, 1295 (2017).

44. De Luca, A., Carotenuto, A., Rachiglio, A., Gallo, M., Maiello, M. R., Aldinucci, D. et al. The role of the EGFR signaling in tumor microenvironment. *J. Cell. Physiol.* **214**, 559–567 (2008).

45. Yu, X., Li, W., Deng, Q., You, S., Liu, H., Peng, S. et al. Neoalbaconol inhibits angiogenesis and tumor growth by suppressing EGFR-mediated VEGF production. *Mol. Carcinogenesis* **56**, 1414–1426 (2017).

46. Dittmann, K., Mayer, C., Czemmel, S., Huber, S. M. & Rodemann, H. P. New roles for nuclear EGFR in regulating the stability and translation of mRNAs associated with VEGF signaling. *PLoS ONE* **12**, e0189087 (2017).

47. Lin, B., Song, X., Yang, D., Bai, D., Yao, Y. & Lu, N. A. Anlotinib inhibits angiogenesis via suppressing the activation of VEGFR2, PDGFRβ and FGFR1. *Gene* **654**, 77–86 (2018).

48. Han, B., Li, K., Zhao, Y., Li, B., Cheng, Y., Zhou, J. et al. Anlotinib as a third-line therapy in patients with refractory advanced non-small-cell lung cancer: a multicentre, randomised phase II trial (ALTER0302). *Br. J. Cancer* **118**, 654–661 (2018).

49. Wang, G., Sun, M., Jiang, Y., Zhang, T., Sun, W., Wang, H. et al. Anlotinib, a novel small molecular tyrosine kinase inhibitor, suppresses growth and metastasis via dual blockade of VEGFR2 and MET in osteosarcoma. *Int. J. Cancer* **145**, 979–993 (2019).

50. Tang, L., Yu, W., Wang, Y., Li, H. & Shen, Z. Anlotinib inhibits synovial sarcoma by targeting GINS1: a novel downstream target oncogene in progression of synovial sarcoma. *Clin. Transl. Oncol.* **21**, 1624–1633 (2019).